Journal of Power Sources 232 (2013) 86–92

Contents lists available at SciVerse ScienceDirect

Journal of Power Sources

journal homepage: www.elsevier.com/locate/jpowsour

Construction of NiCo–Pt nanopolyhedron inlay-structures and their highly efficient catalysis hydrolytic dehydrogenation toward ammonia borane

Ming Wen [a,b,*], Shiqing Zhou [b], Qingsheng Wu [a,b], Juyang Zhang [b], Qingnan Wu [b], Chenxiang Wang [b], Yuzhen Sun [b]

[a] Department of Chemistry, Tongji University, 1239 Siping Road, Shanghai, China
[b] Key Laboratory of Yangtze River Water Environment, Ministry of Education, Tongji University, 1239 Siping Road, Shanghai 200092, China

HIGHLIGHTS

- New designed NiCo–Pt nanopolyhedron inlay-structures have been firstly reported in this work.
- NiCo–Pt hexagonal-nanoplates exhibit exceedingly high dehydrogenation catalytic activity.
- NiCo–Pt magnetic nanopolyhedrons can be separated and recovered for recyclable use.
- As-obtained NiCo–Pt nanopolyhedrons have the potential application in energy source.

GRAPHICAL ABSTRACT

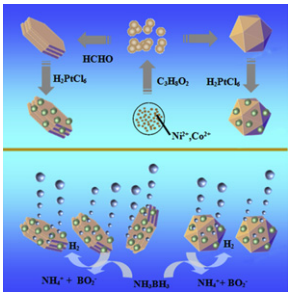

ARTICLE INFO

Article history:
Received 16 July 2012
Received in revised form
14 December 2012
Accepted 17 December 2012
Available online 9 January 2013

Keywords:
NiCo–Pt nanopolyhedrons
Inlay-structures
Catalysis
Dehydrogenation
Ammonia borane

ABSTRACT

New NiCo–Pt nanopolyhedron inlay-structures with an average diameter of ~450 nm have been synthesized through replacement deposition Co or Ni by reductive replacement with a Pt submonolayer (galvanic replacement) on NiCo hexagonal nanoplates and nanoicosahedrons. The resultant products are investigated as hydrolytic dehydrogenation catalyst for potential hydrogen energy applications. The NiCo–Pt nanopolyhedrons exhibit higher catalytic activity than NiCo nanopolyhedrons for the hydrolysis of borane in aqueous ammonia borane at ambient atmosphere and room temperature. In particular, the NiCo–Pt hexagonal nanoplates exhibit efficient catalytic activity with a lower activation energy of 45.72 kJ mol^{-1} than that (49.4 kJ mol^{-1}) for NiCo.

© 2012 Elsevier B.V. All rights reserved.

1. Introduction

Hydrogen, one of most ideal and cleanest energy sources, is a great contender for a leading energy sources in the future for environmental benigancy and sustainable development [1–4]. Thus, having attracted much attention, practical application of hydrogen has been identified as a core subject. Recent reports illustrate that ammonia borane (AB) has a hydrogen capacity of 19.6 wt%, which is

* Corresponding author. Key Laboratory of Yangtze River Water Environment, Ministry of Education, Tongji University, 1239 Siping Road, Shanghai 200092, China. Tel.: +86 21 65982653x8544; fax: +86 21 65981097.
E-mail address: m_wen@tongji.edu.cn (M. Wen).

0378-7753/$ – see front matter © 2012 Elsevier B.V. All rights reserved.
http://dx.doi.org/10.1016/j.jpowsour.2012.12.070

much higher than gasoline. Therefore, it is widely appraised as a promising candidate for effective hydrogen storage medium [5–11]. To efficiently release hydrogen from storage medium, including AB, it is of great significance to develop economical catalysts with long cycle life to release hydrogen under moderate conditions [12]. Considered as quasi-homogeneous systems, nanocatalysts can achieve high activity and selectivity, which are close to those of homogeneous catalysts. Furthermore, owing to the synergistic effect between two metals, various bimetallic core–shell and alloy nanoparticles (NPs), such as Pt–Ni, Au–Co, Ru–Ni, and Rh–Ni–graphene, exhibit extraordinary catalytic activity for AB dehydrogenation compared to individual NPs [13–18]. However, the stability and efficiency of catalysts are still obstacles, urgent to be addressed.

On the other hand, the area of efficient active crystal surface plays a crucial role in highly catalysis activity. Since the exposed efficient active crystal surface is related to the shape of nanomaterials, it is possible to develop high active catalysts only by shape control of the particles [19–21]. Therefore, exploring an approach to increase the area of heterostructured efficient active crystal surface will get high active catalysts for the dehydrogenation of AB. But it still remains a challenge for the controlling synthesis of nano-catalyst with high proportional active crystal surface, especially for that of heterostructured alloy nanocatalyst. Through the cooperation of component mediated electron structure and high efficient catalytic surface atomic arrangement, heterostructured alloy nano-catalysts can finely tune the catalytic performance [22–26]. Thus, the construction of uniform heteronanostructured alloy nanopolyhedron with high proportional active crystal surface will evidently improve the catalysis reactivity.

In this work, we first report on the construction of new uniform NiCo–Pt inlay-structured polyhedron nanocatalysts, in which Pt nanoparticles were well distributed on the surface of NiCo alloy nanoicosahedrons and hexagonal nanoplates. To examine the morphologies, structures and properties of as-synthesized samples, the characterization was carried out by X-ray diffraction (XRD), high resolution transmission electron microscopy (HRTEM), scanning electron microscopy (SEM) and vibration sample magnetometry (VSM). Compared with NiCo nanopolyhedrons, the catalytic activity of hydrolytic dehydrogenation toward AB can be remarkably enhanced by the heterostructured NiCo–Pt nanopolyhedrons inlay-structure under ambient atmosphere at room temperature (r.t.). Especially, NiCo–Pt hexagonal nanoplates, with high efficient catalytic activity and long-term stability, can be valuable for the potential application in energy source and chemical industry.

2. Experimental

2.1. Chemicals

Ammonia-borane (AB, NH_3BH_3, 90%) was purchased from Aldrich, $Ni(AC)_2{\cdot}4H_2O$ (99%), $Co(AC)_2{\cdot}4H_2O$ (99%), dihydrogen hexachloroplatinate ($H_2PtCl_6{\cdot}6H_2O$, 99%), NaOH (99%) and polyvinylpyrrolidone K-30 (PVP, $(C_6H_9NO)_n$, Mw: av. 40,000), citric acid ($C_6H_8O_7$,99%), ethyl ethanol (C_2H_5OH, 99%), propylene glycol

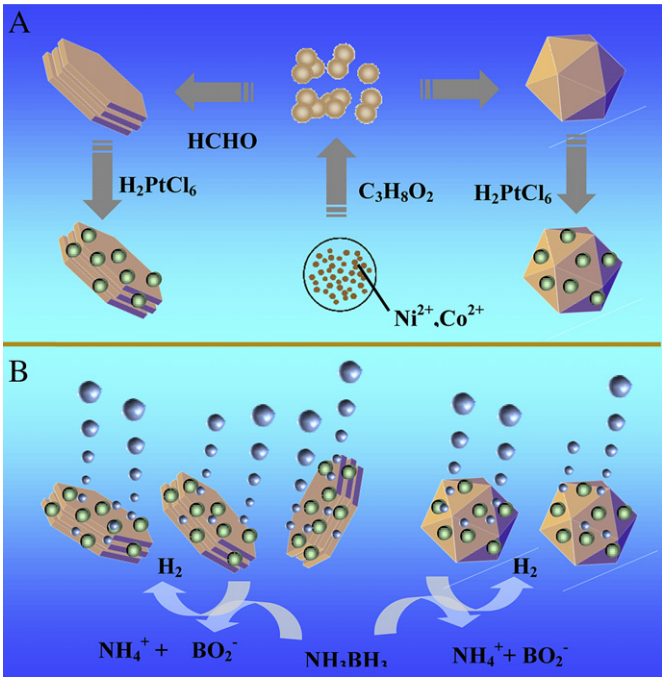

Scheme 1. (A) Formation process of NiCo–Pt nanopolyhedron inlay-structures; (B) the schematic view of hydrolytic dehydrogenation toward AB.

($C_3H_8O_2$, 99%) were purchased from Sinopharm Chemical Reagent Co., Ltd (SCRC), and were used without further purification.

2.2. Preparation of NiCo nanopolyhedrons

In a typical synthesis experiment of NiCo hexagonal plates nanocatalysts, 2 mL ethyl alcohol was mixed with 500 μL $Ni(AC)_2{\cdot}4H_2O$ aqueous solution (0.12 M), 500 μL $Co(AC)_2{\cdot}4H_2O$ aqueous solution (0.12 M), 1 mL NaOH aqueous solution (1.2 M) at room temperature. The mixture was dissolved by ultrasonic. 7 mL propylene glycol and 70 μL HCHO were injected and the mixture was maintained in the autoclave. To avoid the oxidation of products in the existence of atmospheric oxygen, high-purity argon was bubbled through the solution, and then the autoclave was sealed and maintained at 200 °C for 10 h. The resulting products were collected by centrifugation and washed several times with distilled water and ethanol, then were dried for the following experiment. NiCo icosahedrons nanocatalysts were synthesized under the above same condition but without methanol.

2.3. Preparation of NiCo–Pt nanopolyhedrons

The synthesis of NiCo–Pt hexagonal nanoplates and nanoicosahedrons were achieved through galvanic replacement process between Pt and Ni or Co on the surface of NiCo hexagonal nanoplates and nanoicosahedrons using citric acid as capping agents. Briefly, 10 mg of the as-synthesized NiCo hexagonal

Table 1
Saturation magnetization (Ms) and coercivity (Hc) of NiCo nanopolyhedrons and inlay-structured NiCo–Pt nanopolyhedrons.

Sample no.	Initial molar ratio (Ni^{2+}:Co^{2+}:Pt^2)	Alloy content (at.%)	Ms (emu g^{-1})	Hc (Oe)
S1 (NiCo nanoicosahedrons)	50:50	$Ni_{50}Co_{50}$	128.82	133.61
S2 (NiCo hexagonal nanoplates)	50:50	$Ni_{50}Co_{50}$	110.29	132.80
S3 (NiCo–Pt nanoicosahedrons)	48:48:4	$Ni_{47}Co_{40}$–Pt_{13}	104.05	131.25
S4 (NiCo–Pt hexagonal nanoplates)	48:48:4	$Ni_{47}Co_{39}$–Pt_{14}	89.69	118.12

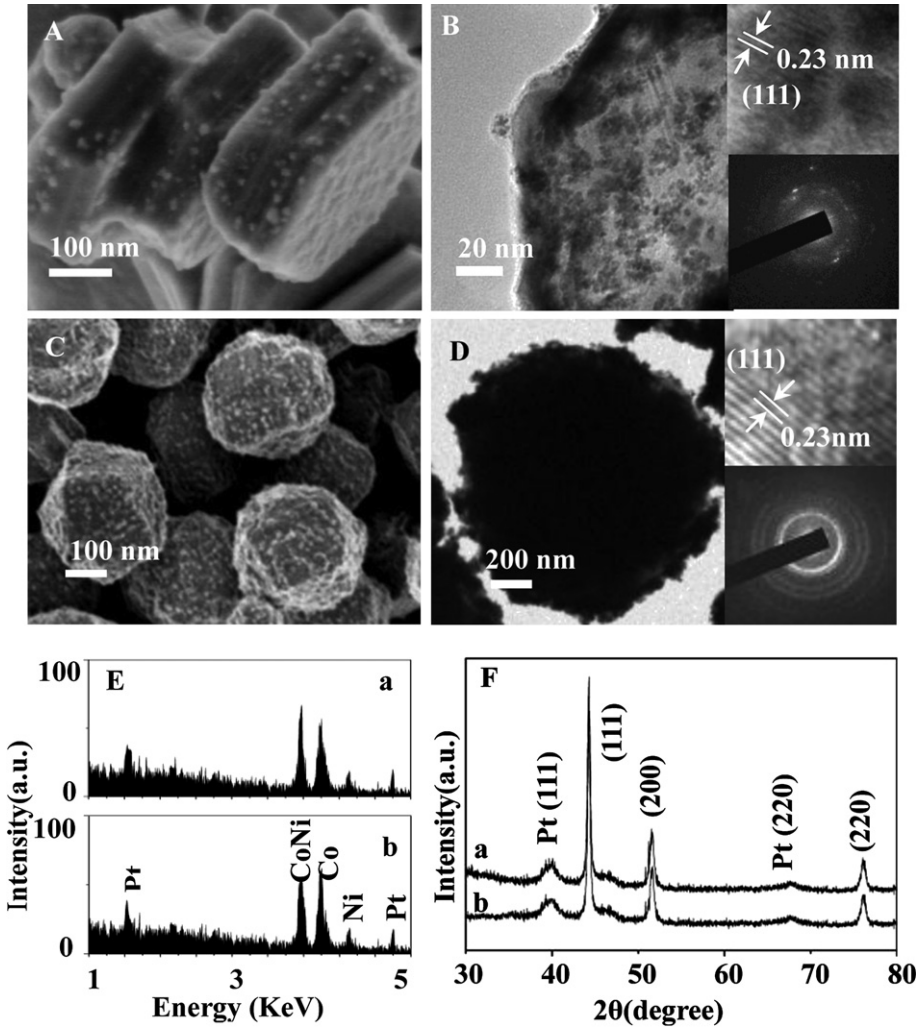

Fig. 1. (A) SEM and (B) TEM images of NiCo–Pt hexagonal nanoplates with inset HRTEM above and SADP below; (C) SEM and (D) TEM images of NiCo–Pt nanoicosahedrons with inset HRTEM above and SADP below; (E) EDS of NiCo–Pt hexagonal nanoplates (a) and nanoicosahedrons (b); (F) XRD patterns of NiCo–Pt hexagonal nanoplates (a) and nanoicosahedrons (b).

nanoplates and icosahedrons were dispersed in the 40 mL mixed solvent of ethanol (20 mL) and deionized water (20 mL), then 2 mL $H_2PtCl_6 \cdot 6H_2O$ aqueous solution (3 mM) and 2 mL citric acid (6 mM) were added in the above mixture solution by ultrasonic. After 15 min, suspension solution was collected, centrifuged timely and washed by distilled water and ethanol. At last, dry the products for the following dehydrogenation catalysis test. The components of resultant NiCo–Pt hexagonal nanoplates and nanoicosahedrons measured by atomic absorption spectrometer (AAS) are $Ni_{47}Co_{39}$–Pt_{14} and $Ni_{47}Co_{40}$–Pt_{13}, respectively.

2.4. Hydrolytic dehydrogenation catalysis evaluation

To study the catalytic property of the as-synthesized products, we evaluated their catalytic activities for the hydrolytic dehydrogenation of borohydride aqueous. In a typical experiment, 15 mL of AB (0.13 M, pH >8) and KBH_4 solution (0.13 M, pH >8), 15 mL deionized water was added to a three-necked round-bottom flask (one neck was connected to a gas burette through soft rubber tube, and the other was connected to temperature control device). Then catalysts (45.0 mg NiCo hexagonal nanoplates, 45.0 mg NiCo nanoicosahedrons, 45.0 mg NiCo–Pt hexagonal nanoplates, 45.0 mg NiCo–Pt nanoicosahedrons) were added into the reaction solution rapidly and every pipe orifice was kept sealed. The reaction was started and preceded under constant electric stirring at 30 °C. The volume of hydrogen gas generated from the hydrolysis reaction was measured by the water-displacement method.

2.5. Characterization measurements

The morphology and size of as-synthesized samples were determined by employing Hitachi S-4800 scanning electron microscopy (FE-SEM), JEOL JEM-1200EX (Japan) transmission electron microscopy (TEM) and high resolution transmission electron microscopy (HRTEM). Selected area energy dispersive X-ray spectroscopy (EDXS) was conducted at 20 keV on a TN5400 EDS instrument (Oxford), and all samples were handled under air atmosphere. Alloy element analysis of Ni, Co and Pt was measured at $\lambda = 232.0$ nm, 240.7 nm and 265.9 nm respectively, by graphite furnace AAS (6810, Shanghai Chromatogram Technology Company, China). The powder X-ray diffraction analysis (XRD) patterns were recorded using Bruker D8 (German) diffractometer with a Cu Kα X-ray radiation source ($\lambda = 0.154056$ nm). X-ray photoelectron spectroscopy (XPS) experiments were carried out on a RBD upgraded PHI-5000C ESCA system (Perkin Elmer) with Al Kα radiation ($h\nu = 1486.6$ eV). The whole spectra (0–1100 eV) and the

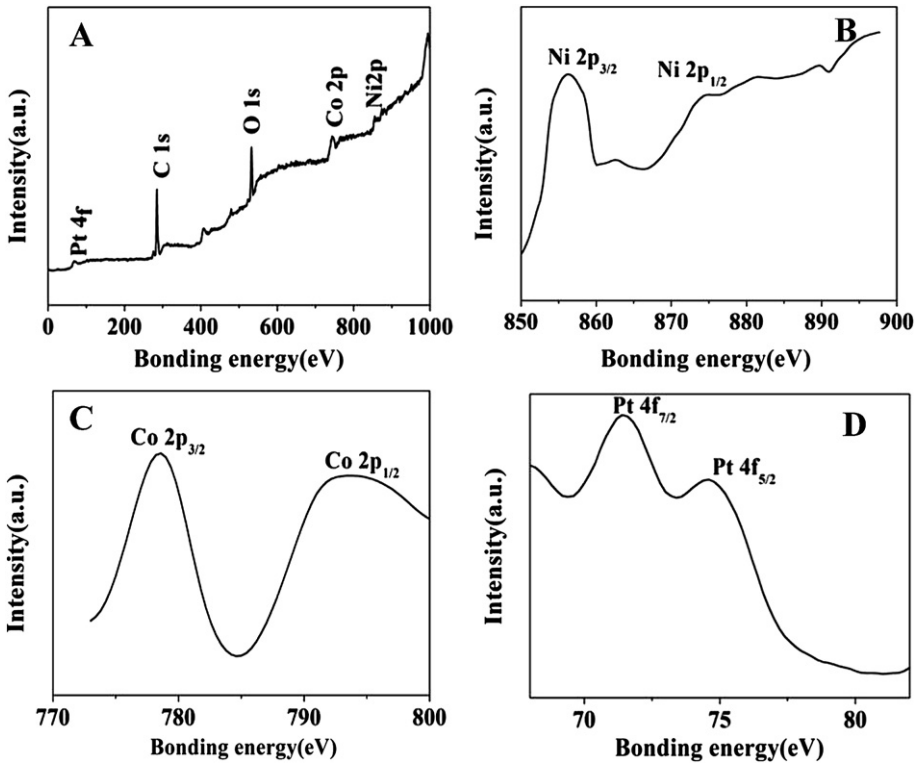

Fig. 2. (A) XPS spectra; (B–D) detailed spectra of Ni 2*p*, Co 2*p* and Pt 4*f* for NiCo–Pt hexagonal nanoplates. All the horizontal axes represent the binding energy corrected by that of C 1s.

narrow spectra of all the elements with much high resolution were both recorded by using RBD 147 interface (RBD Enterprises USA) through the AugerScan 3.21 software. Binding energies were calibrated by using the containment carbon (C1s = 288.174 eV). The data analysis was carried out by using the RBD AugerScan 3.21 software provided by RBD Enterprises or XPSPeak4.1 provided by Raymund W.M. Kwok (The Chinese University of Hongkong, China). Vibration sample magnetometry (VSM) was used to examine the magnetic properties on lakeshore7312, and the data are summarized in Table 1.

3. Results and discussion

3.1. Construction mechanism of NiCo–Pt nanopolyhedron inlay-structures

For improving catalytic activity, herein we report on the construction of new designed NiCo–Pt nanopolyhedron inlay-structures through galvanic replacement process using NiCo hexagonal nanoplates and nanoicosahedrons as sacrificial templates (shown in Scheme 1A). The NiCo alloy hexagonal nanoplates and nanoicosahedrons were obtained via the controlling growth process of methanal molecular. Firstly, Ni^{2+} and Co^{2+} were reduced by propylene glycol and alloyed. Owing to the selective absorption controlling of methanal molecular on different NiCo crystal facets [27,28], NiCo alloy hexagonal nanoplates were readily prepared by introducing methanal with concentration of 0.07 ml, while nanoicosahedrons were obtained in the absence of methanol; Then NiCo hexagonal nanoplates or nanoicosahedrons were added to $PtCl_6^{2-}$ solution in the presence of citrate acid, $PtCl_6^{2-}$ were reduced and deposited as well-distribution Pt NPs inlaid the surface of NiCo nanopolyhedrons, because the standard reduction potentials (SHE) of the $PtCl_6^{2-}$/Pt redox couple (0.735 V) are much higher than that of the Co^{2+}/Co redox couple (−0.277 V) and Ni^{2+}/Ni redox couple (−0.246 V); finally, the process resulted in NiCo–Pt nanopolyhedrons inlay-structures via the control of reaction time and concentration of $PtCl_6^{2-}$. Notably, when these NiCo–Pt inlay-heterostructures are employed as dehydrogenation catalysts, the activity of catalytic dehydrogenation toward AB is remarkably enhanced under ambient atmosphere at r.t. compared to NiCo nanopolyhedrons, promising the potential application in energy source and chemical industry.

3.2. Characterization of NiCo–Pt inlay-structured nanopolyhedrons

Fig. 1 shows inlay-structured NiCo–Pt nanopolyhedrons. In Fig. 1A and C, the average diameters of hexagonal nanoplates and nanoicosahedrons are ~380 (SI, Figure S1) and ~450 nm with

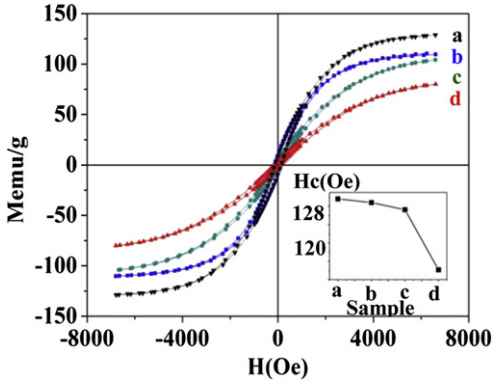

Fig. 3. Room-temperature hysteresis loops of (a) NiCo nanoicosahedrons, (b) NiCo hexagonal nanoplates, (c) NiCo–Pt nanoicosahedrons, and (d) NiCo–Pt hexagonal nanoplates (inset: the corresponding coercivity variation).

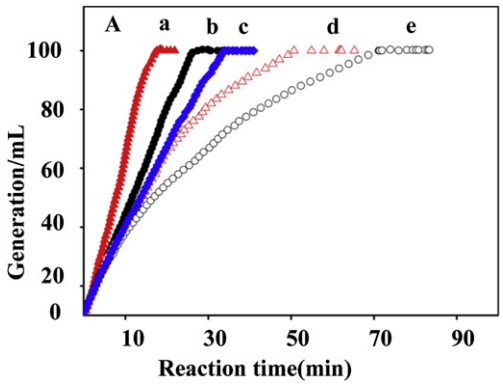

Fig. 4. (A) Hydrogen generation from AB aqueous (0.13 M, 20 mL) catalyzed by (a) NiCo–Pt hexagonal nanoplates, (b) NiCo–Pt nanoicosahedrons, (c) Pt NPs, (d) NiCo hexagonal nanoplates, (e) NiCo nanoicosahedrons.

inlaid-Pt-NPs size of ~10 nm, respectively. TEM images clearly illustrate that each Pt NP consists of small nucleus (~3 nm) (Fig. 1B and D). Inset Fig. 1B and D, HRTEM image of Pt NPs has mainly lattice spacing's of 0.23 nm, corresponding to (111) planes in Pt face-center-cubic (fcc) structure, while its SAED pattern presents clear crystalline spot ring, indicating that Pt is isolated and inlays the surface of NiCo nanopolyhedrons. Additionally, EDS performed on inlay-structured NiCo–Pt hexagonal nanoplates and nanoicosahedrons undoubtedly indicate they consist of Ni, Co and Pt with atomic ratio of Ni:Co:Pt at ~3:3:1 (Fig. 1E). XRD patterns of NiCo–Pt nanopolyhedrons are given in Fig. 1F. The diffraction peaks could be indexed to those of either Ni or Co and Pt fcc structure (JCPDS No. 01-1260 & 15-0806 & 01-1194).

The formation of NiCo–Pt nanopolyhedron inlay-structures is confirmed by XPS. Fig. 2A illustrates XPS analysis on the surface of NiCo–Pt inlay-structured hexagonal nanoplates. The photoemission peaks of Pt4*f*, C1*s*, O1*s*, Co2*p*, Ni2*p* can be observed. Magnified Ni2*p* peaks in Fig. 2B consist of two sharp peaks 854.4 and 871.2 eV due to the spin–orbit splitting of $2p_{3/2}$ and $2p_{1/2}$, agreeing with Ni(II) and Ni(0). For Co 2*p*, two peaks resulted by the 2*p* electrons multiplet-splitting are $2p_{3/2}$ and $2p_{1/2}$ with BE values of 778 and 793.2 eV, implying for Co(II) and Co(0) (Fig. 2C). In Fig. 2D, detailed spectra of Pt are composed of two peaks of 71.4 and 74.6 eV owing to the spin–orbit doublet splitting of $4f_{7/2}$ and $4f_{5/2}$, indicating that Pt(0) is dominant. The O 1*s* peak of 532.7 eV implied that oxygen (O^{2-}) species (oxides of nickel and cobalt) existed on NPs surface. Because the environment of Ni, Co and Pt in resultant

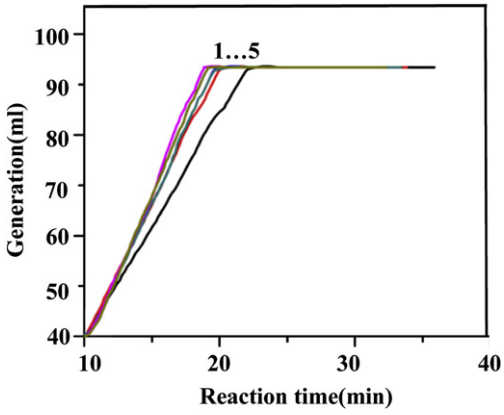

Fig. 5. Hydrogen generation from above AB aqueous solution catalyzed by NiCo hexagonal nanoplates from the 1st to 5th run of the lifetime experiment under ambient atmosphere at room temperature. Catalyst/AB = 0.0146 (molar ratio).

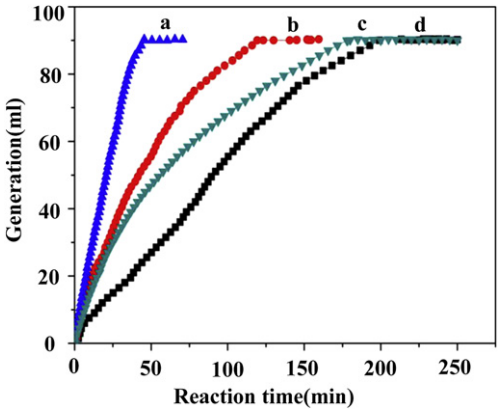

Fig. 6. Hydrogen generation from KBH_4 aqueous solution (15 mL, containing 0.45 wt% NaOH and 0.56 wt% KBH_4) catalyzed by NiCo–Pt hexagonal nanoplates (a), NiCo–Pt nanoicosahedrons (b), NiCo hexagonal nanoplates (c), and NiCo nanoicosahedrons (d) under ambient atmosphere at room temperature. Catalyst/KBH_4 = 0.0146 (molar ratio).

inlay-structured NiCo–Pt nanopolyhedrons is different from their pure metals, their XPS peaks are slightly shift compare to those in Binding Energy Lookup Table [29]. The similar case can be observed in NiCo–Pt nanoicosahedron inlay-structures (SI, Figure S2).

3.3. Magnetic property

Fig. 3 plots the magnetization versus applied field for NiCo–Pt and NiCo nanopolyhedrons. The detail data are summarized in Table 1. The saturation magnetization (Ms) of NiCo–Pt nanopolyhedrons is lower than that of NiCo nanopolyhedrons, in which Ms of hexagonal nanoplates shaped NiCo–Pt and NiCo at 89.69 emu g^{-1} and 110.29 emu g^{-1} are lower than that of nanoicosahedrons shaped NiCo–Pt and NiCo at 104.05 emu g^{-1} and 128.82 emu g^{-1}, respectively. The coercivity (Hc) for NiCo–Pt and as-contrast NiCo nanopolyhedrons are inset in Fig. 3. The variation trend of Hc follows that of Ms, in which Hc of NiCo nanoicosahedrons and hexagonal nanoplates at 133.61 and 132.80 Oe are slightly higher than those (131.25 and 118.12 Oe) of NiCo–Pt nanoicosahedrons and hexagonal nanoplates. In addition, the as-prepared inlay-structured NiCo–Pt hexagonal nanoplates can be easily separated and recovered by an external magnetic field (SI, Figure S3). Thus, the magnetic behavior can be changed by shape and inlay-heterostructures.

4. Hydrolytic dehydrogenation catalytic activity

The hydrolysis of NH_3BH_3 can be briefly expressed as follows:

$$NH_3BH_3(aq) + 2H_2O \xrightarrow{\text{Catalysts}} NH_4^+(aq) + BO_2^-(aq) + 3H_2(g) \quad (1)$$

Only borane, but not ammonia, is dehydrogenated in this hydrolysis process. It is observed an equilibrium process and a rapid change between boracic compounds such as BO_2^-, H_3BO_3, and other borate species. Thus, BO_2^- would not interfere with hydrogen generation in a hydrolysis reactor of borane [14,30,31]. Because H_2 liberation efficiency can be significantly enhanced by suitable catalysts, the catalytic activity of resultant inlay-structured NiCo–Pt nanopolyhedrons for hydrolysis dehydrogenation toward AB aqueous has been investigated. Fig. 4 shows the amount of hydrogen generated as a function of reaction time by different as-prepared catalysts. In Fig. 4, NiCo–Pt nanopolyhedrons inlay-structures exert remarkable catalytic activity of hydrolytic dehydrogenation toward AB aqueous compared to NiCo

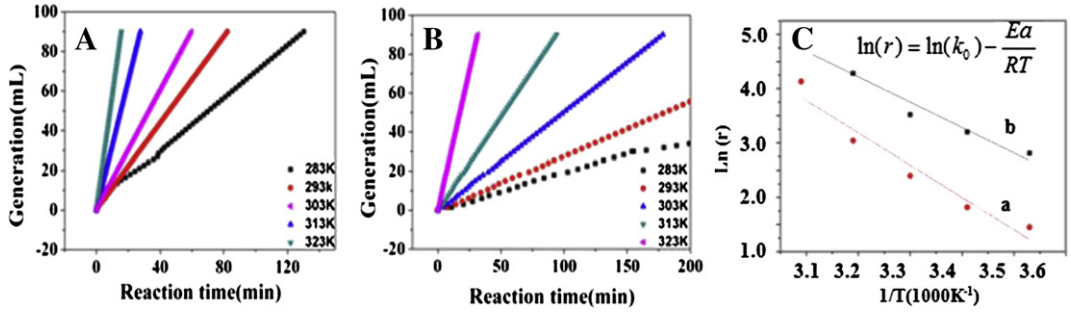

Fig. 7. Hydrogen generation from AB aqueous solution (0.13 M, 20 mL) catalyzed by NiCo–Pt hexagonal nanoplates (A) and NiCo (B) in reaction temperatures at 283, 293, 303, 313 and 323 K (from the right to the left side); (C) Arrhenius plot for dehydrogenation of AB aqueous using NiCo–Pt (a) and NiCo (b) hexagonal nanoplates as catalysts. (In the inserted equation, r represents the reaction rate (ml min^{-1} g^{-1}), k_0 the reaction constant (mol min^{-1} g^{-1}), Ea the activation energy of the reaction (kJ mol^{-1}), R the universal gas constant, and T (K) the reaction temperature.)

nanopolyhedrons and Pt NPs, in which NiCo–Pt hexagonal nanoplates complete dehydrogenation of AB in 19 min (curve (a)), is quicker than NiCo–Pt nano-icosahedrons in 28 min (curve (b)). The hydrolytic dehydrogenation time of 50 min catalyzed by NiCo hexagonal nanoplates (curve (d)) is shorter than that (71 min) by NiCo nanoicosahedrons (curve (e)). So the hydrolytic dehydrogenation catalytic activity of resultant catalysts depended on shape and can be markedly enhanced by inlaid-Pt NPs. This excellent catalytic activity, possibly due to the combination of strain and ligand effects at interface between inlaid-Pt and exposed active crystal plane of NiCo, may change the width of the surface d-band of Ni and Co. Because the d-band width is closely related to the interatomic matrix element that describes the bonding interactions between d orbital and its nearest neighbors, several chemical properties, e.g. the dissociative adsorption energy of hydrogen is influenced by varied induced average energy of the d-band through width modification [30–33]. Consequently, the cooperation between high proportional active crystal surface of hexagonal nanoplates and NiCo–Pt inlay-heterostructures results in the excellent hydrolysis dehydrogenation, which is more than that of NiCo–Pt nano-icosahedrons because of the higher proportional of exposed area of active crystal plane at 28.21 × 106 m^2 for hexagonal nanoplates, compare to 6.81 × 106 m^2 for nanoicosahedrons in the unit volume (per m^3) (Scheme 1B).

The lifetime and stability is important factors for catalyst application, the catalytic activity of inlay-structured NiCo–Pt hexagonal nanoplates has been tested for five times for hydrolytic dehydrogenation toward AB aqueous under ambient atmosphere at room temperature. Fig. 5 shows the hydrogen generation from above AB aqueous solution catalyzed by inlay-structured NiCo–Pt hexagonal nanoplates from the 1st to 5th run of the lifetime experiment under ambient atmosphere at room temperature. Only the small decrease (17%) of catalytic activity for the NiCo–Pt hexagonal nanoplates can be observed over five times tests. The reaction time increased from 19 min to 23 min from the first to the fifth.

Additionally, it also exhibits excellent catalytic activity for the hydrogen generation in KBH_4 aqueous. When catalysts are added, the release of hydrogen is rapid via the following reaction:

$$K^+ + BH_4^- + 2H_2O \rightarrow K^+ + BO_2^- + 4H_2\uparrow \quad (2)$$

Fig. 6 presents the amount of hydrogen generated as a function of reaction time by employing different as-obtained catalysts. Compared to NiCo nanopolyhedrons, NiCo–Pt inlay-heterostructured nanopolyhedrons exhibit markedly high catalytic activity. In particular, NiCo–Pt hexagonal nanoplates can complete dehydrogenation reaction of KBH_4 aqueous within 40 min (curve (a)), which is much higher than that of NiCo–Pt nanoicosahedrons (curve (b), 120 min) and NiCo nanopolyhedrons (curve (c), 170 min for NiCo hexagonal nanoplates; curve (d), 200 min for NiCo nanoicosahedrons). Hence, this magnetic high performance catalyst can be easily recovered by an external magnet based on its long lifetime and stability. Therefore, the as-designed NiCo–Pt hexagonal nanoplates have the good lifetime and stability for the hydrolytic hydrogen generation of AB under ambient atmosphere at r.t.

In dehydrogenation process, temperature is very important and was investigated for the catalytic dehydrogenation rates of NiCo–Pt and NiCo hexagonal nanoplates toward AB aqueous (0.13 M) with the molar ratio of catalyst/AB of 0.0146. When temperature increases from 283 to 323 K, the generation rate of H_2 rises substantially from 15 to 128 mL min^{-1} g^{-1} for NiCo–Pt (Fig. 7A) and from 4 to 64 mL min^{-1} g^{-1} for NiCo (Fig. 7B). Since the amount of H_2 generated is linearly dependent on reaction time at each temperature, it demonstrates that such a dehydrogenation reaction is zero order [34]. Using NiCo–Pt hexagonal nanoplates as catalyst, the activation energy of the dehydrogenation of AB aqueous can be calculated by the Arrhenius equation in a zero-order reaction. Fig. 7C plots the Arrhenius plot of ln(r) versus 1/T. The activation energy is estimated to be 45.72 kJ mol^{-1} for NiCo–Pt (line (a)), which is lower than that (49.4 kJ mol^{-1}) for NiCo (line (b)), and is lower than that of many unitary and bimetallic catalysts [14,15,33–36].

5. Conclusion

In conclusion, new designed nanocatalysts of NiCo–Pt nanopolyhedron inlay-structures have been synthesized through galvanic replacement deposition of inlaid-Pt on the surface of NiCo hexagonal nanoplates and icosahedrons. The cooperation between high proportional active crystal surface areas of hexagonal nanoplates and NiCo–Pt inlay-heterostructures results in the excellent dehydrogenation catalytic activity with low activation energy toward AB aqueous under ambient atmosphere at room temperature, suggesting the potential application in energy source and chemical industry as new catalysts.

Acknowledgments

This work was financially supported by the National Natural Science Foundation of China (Nos: 21171130, 51271132, 91222103, 51072134 and 91122025), and 973 Project of China (No: 2011CB932404).

Appendix A. Supplementary data

Supplementary data related to this article can be found in the online version, at http://dx.doi.org/10.1016/j.jpowsour.2012.12.070.

References

[1] W. Grochala, P.P. Edwards, Chem. Rev. 104 (2004) 1283.
[2] P. Chen, Z. Xiong, J. Luo, J. Lin, K.L. Tan, Nature 420 (2002) 302.
[3] Schlapbach, A. Zuttel, Nature 414 (2001) 353.
[4] J.M. Ogden, Rev. Energy Environ. 24 (1999) 227.
[5] A. Gutowska, L.Y. Li, Y.S. Shin, C.M.M. Wang, X.H.S. Li, J.C. Linehan, R.S. Smith, B.D. Kay, B. Schmid, W. Shaw, M. Gutowski, T. Autrey, Angew. Chem. Int. Ed. 4 (2005) 3578.
[6] Y.S. Chen, J.L. Fulton, J.C. Linehan, T. Autrey, J. Am. Chem. Soc. 27 (2005) 3254.
[7] D.W. Himmelberger, C.W. Yoon, M.E. Bluhm, P.J. Carroll, L.G. Sneddon, J. Am. Chem. Soc. 131 (2009) 14101.
[8] B.L. Davis, D.A. Dixon, E.B. Garner, J.C. Gordon, M.H. Matus, B. Scott, F.H. Stephens, Angew. Chem. Int. Ed. 48 (2009) 6812.
[9] R.J. Keaton, J.M. Blacquiere, R.T. Baker, J. Am. Chem. Soc. 129 (2007) 1844. M.E. Bluhm, M.G. Bradley, R. Butterick, U. Kusari, L.G. Sneddon, J. Am. Chem. Soc. 128 (2006) 7748.
[10] T.B. Marder, Angew. Chem. 119 (2007) 8262.
[11] M. Wen, D. Yang, Q.S. Wu, R.P. Lu, Y.Z. Zhu, F. Zhang, Chem. Commun. 46 (2010) 219.
[12] J.M. Yan, X.B. Zhang, S. Han, H. Shioyama, Q. Xu, Angew. Chem. Int. Ed. 46 (2007) 8153.
[13] J. Wang, X.B. Zhang, Z.L. Wang, L.M. Wang, Y. Zhang, Energy Environ. Sci. 10 (2012) 1039.
[14] M. Chandra, Q. Xu, J. Power Sources 168 (2007) 135.
[15] H.Z. Guo, Y.Z. Chen, X.Z. Chen, R.T. Wen, G.H. Yue, D.L. Peng, Nanotechnology 22 (2011) 195604.
[16] X.J. Yang, F.Y. Cheng, J. Liang, Z.L. Tao, J. Chen, Int. J. Hydrogen Energy 34 (2009) 8785.
[17] H.L. Jiang, T. Umegaki, T. Ajita, X.B. Zhang, M. Haruta, Q. Xu, Chem. Eur. J. 16 (2010) 3132.
[18] G. Chen, S. Desinan, R. Nechache, R. Rosei, F. Rosei, D. Ma, Chem. Commun. 47 (2011) 6308.
[19] M.A. Mahmoud, C. Tabor, E.Y. Ding, Z.L. Wang, M.A. El-Sayed, J. Am. Chem. Soc. 130 (2008) 4590.
[20] H. Lee, S.E. Habas, S. Kweskin, D. Butcher, G.A. Somorjai, P. Yang, Angew. Chem. 118 (2006) 7988.
[21] S.M. Davis, F. Zaera, G.A. Somorjai, J. Catal. 85 (1984) 206.
[22] M. Wen, B.L. Sun, B. Zhou, Q.S. Wu, J. Peng, J. Mater. Chem. 22 (2012) 11988.
[23] B.L. Sun, M. Wen, Q.S. Wu, J. Peng, Adv. Funct. Mater. 22 (2012) 2860.
[24] K.B. Zhou, X. Wang, X.M. Sun, Q. Peng, Y.D. Li, J. Catal. 229 (2005) 206.
[25] S.Q. Zhou, M. Wen, N. Wang, Q.S. Wu, Q.N. Wu, L.Y. Cheng, J. Mater. Chem. 22 (2012) 16858.
[26] H.J. Shin, R. Ryoo, Z. Liu, O. Terasaki, J. Am. Chem. Soc. 123 (2001) 1246.
[27] T.K.N. Hoang, L. Deriemaeker, V.B. Finsy, R. La, Langmuir 20 (2004) 8966.
[28] X.Q. Huang, S.H. Tang, N.F. Zheng, J. Am. Chem. Soc. 131 (2009) 13916.
[29] B.V. Crist, On-Screen PDF Handbook of Monochromatic XPS Spectra, , In: The Elements and Native Oxides, vol. 1, XPS International, Inc, 1999.
[30] F.Y. Cheng, H. Ma, Y.M. Li, J. Chen, Inorg. Chem. 46 (2007) 788.
[31] D.F. Gaines, R. Schaeffer, J. Am. Chem. Soc. 86 (1964) 1505.
[32] J.R. Kitchin, J.K. Norskov, M.A. Barteau, J.G. Chen, Phys. Rev. Lett. 93 (2004) 156801.
[33] F. Tao, M.E. Grass, Y.W. Zhang, D.R. Butcher, J.R. Renzas, Z. Liu, J.Y. Chung, B.S. Mun, M. Salmeron, G.A. Somorjai, Science 322 (2008) 932.
[34] C.H. Liu, B.H. Chen, C.L. Hsueh, J.R. Ku, S.M. Jeng, F. Tsau, Int. J. Hydrogen Energy 34 (2009) 2153.
[35] J.C. Ingersoll, N. Mani, J.C. Thenmozhiyal, A.J. Muthaiah, J. Power Sources 173 (2007) 450.
[36] S.C. Amendola, S.L. Sharp-Goldman, M.S. Janjua, N.C. Spencer, M.T. Kelly, P.J. Petillo, M. Binder, Int. J. Hydrogen Energy 25 (2000) 969.